Surface localized phonon modes at the Si(553)-Au nanowire system

Julian Plaickner,[1,2,*] Eugen Speiser,[1] Christian Braun,[3] Wolf Gero Schmidt,[3] Norbert Esser,[1,4] and Simone Sanna[5,†]

[1]*Leibniz-Institut für Analytische Wissenschaften-ISAS-e.V., Schwarzschildstrasse 8, 12489 Berlin, Germany*
[2]*Helmholtz-Zentrum Berlin für Materialien und Energie GmbH, Hahn-Meitner-Platz 1, 14109 Berlin, Germany*
[3]*Lehrstuhl für Theoretische Materialphysik, Universität Paderborn, 33095 Paderborn, Germany*
[4]*Technische Universität Berlin, Institut für Festkörperphysik, Hardenbergstrasse 36, 10623 Berlin, Germany*
[5]*Institut für Theoretische Physik and Center for Materials Research (LaMa), Justus-Liebig-Universität Gießen, Heinrich-Buff-Ring 16, D-35392 Gießen, Germany*

(Received 15 January 2021; revised 3 March 2021; accepted 19 March 2021; published 30 March 2021)

The vibrational properties of the Si(553)-Au surface are studied by Raman spectroscopy and *ab initio* calculations. A multitude of surface localized phonon modes with wave number below 200 cm^{-1} is experimentally observed, along with two modes at about 400 cm^{-1}. Atomistic models within density functional theory allow to assign the low-energy spectral features to vibrations within the Au chain, while the Raman signatures at higher energies are mostly localized at the Si step edge. The Raman activity of nominally silent modes associated with a large charge transfer between Au chain and Si step edge states is explained by scattering at charge density fluctuations. Temperature-dependent measurements reveal specific mode shifts that are discussed in terms of a recently proposed order-disorder phase transition. The presence of model-specific displacement patterns allows us to identify the structural models compatible with the measured spectra at low and at room temperature.

DOI: 10.1103/PhysRevB.103.115441

I. INTRODUCTION

The reduction of size and dimensionality of metallic objects gives rise to peculiar physical properties. Phenomena such as spin-charge separation, triplet superconductivity, and Luttinger liquid behavior [1–5] motivated a multitude of fundamental studies on low-dimensional physics. In this respect, self assembly of metallic atomic chains on stepped semiconductor surfaces is regarded as a low size limit for long-range ordered nanostructures [6–12]. Several realizations of such wire systems have been reported, that demonstrate their high reproducibility, stability, and tunability [9,13–22]

Thereby, the Si(553)-Au surface is one of the most studied systems, due to a long-standing debate concerning its atomic structure [9,15,16,23–27]. The Si(553) surface is tilted by 12.5° in [11$\bar{2}$] direction with respect to the (111) plane. It features about 14.8 Å wide (111) nanoterraces, separated by steps of double atomic height along the [1$\bar{1}$0] direction. Evaporation of 0.48 ML Au onto this surface generates one Au chain per terrace as shown in Fig. 1. The exact structure of this system has been controversely discussed. Terraces consisting of parallel double Au strands and a Si honeycomb chain as shown in Fig. 1(a), as proposed by Krawiec [16], are a commonly accepted structural motif. However, while the Krawiec model features a planar Si step edge, in the model proposed by Erwin *et al.* [9] and refined by Hafke *et al.* [25] [Figs. 1(b) and 1(c)], the step edge is spin polarized, and every third step edge atom is shifted downwards by 0.3 Å. Recently, Braun *et al.* [26] proposed a diamagnetic, $sp^2 + p$ rehybridized model [Fig. 1(d)], in which every third edge atom is 0.8 Å lower than the others.

As a further peculiar aspect of this system, an order-disorder phase transition below 100 K has been observed [28], which is currently under discussion [27,29]. Recently, the crucial role of two phonons in driving the structural phase transition at the Si(553)-Au surface has been discussed [27]. In detail, the population of these modes leads to a charge transfer between different regions of the Si(553) terraces, which drives a transition from a (5×6)-periodic to a (5×2)-periodic phase. Yet, a comprehensive study of the vibrational properties of the Si(553)-Au surface is still missing.

In this manuscript, we provide a thorough characterization of the surface-localized phonon modes of the Si(553)-Au system, above and below the phase transition temperature. Besides modes with usual temperature related shifts, modes at 41, 83, and 99 cm^{-1} are observed only at low temperatures (30 K, LT), while a mode at 413 cm^{-1} is only observed at room temperature (300 K, RT). To understand the outcome of the Raman experiments, phonon spectra are calculated from DFT-based atomistic simulations. The comparison between theory and experiment allows to assign the measured spectral features to the calculated displacement patterns. The analysis of the vibrational properties allows for structural identification. The spectra calculated for the double Au strand [16] and the $sp^2 + p$ rehybridized [26] models are compatible with the HT and LT measured spectra, respectively.

II. METHODOLOGY

A. Computational details

DFT calculations within the generalized gradient approximation (GGA) in the revised Perdew-Burke-Ernzerhof

*julian.plaickner@helmholtz-berlin.de
†simone.sanna@theo.physik.uni-giessen.de

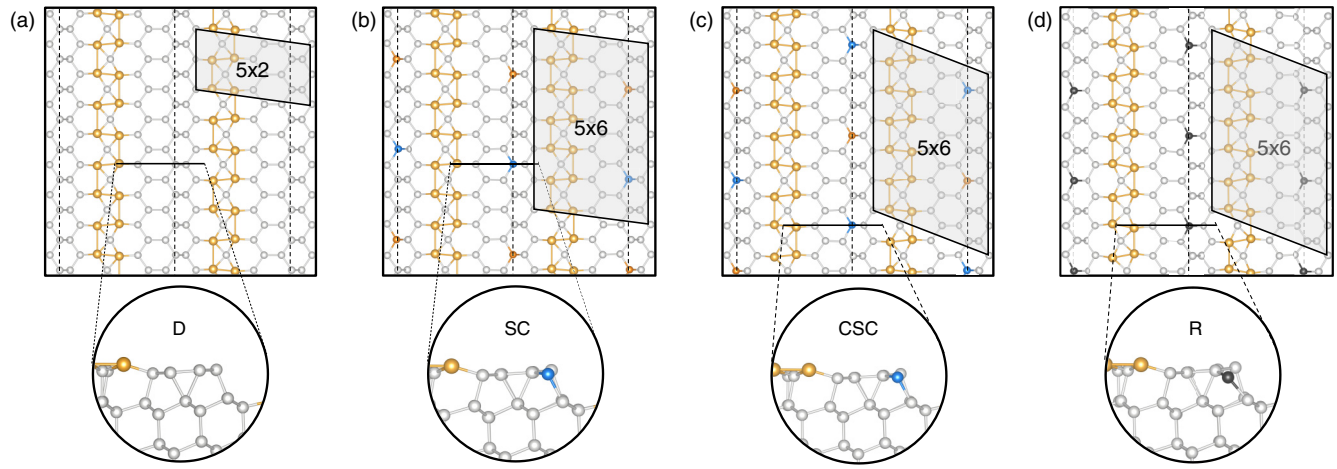

FIG. 1. Structural models of the Si(553)-Au surface. (a) Double Au strand model—D—as proposed by Krawiec[16]. (b) Spin-chain model—SC—proposed by Erwin *et al.* [9] and subsequently refined (c) to a centered spin-chain—CSC—by Hafke *et al.* [25]. Spin-polarized step-edge atoms are represented in blue (spin up) and red (spin down). (d) $sp^2 + p$ rehybridized model (R) as proposed by Braun *et al.* [26]. Si atoms vertically displaced from the step edge are shown in black. Surface unit cells are highlighted.

(PBEsol) formulation [30] have been performed with the Vienna *ab initio* simulation package (VASP) [31,32]. Projector augmented waves (PAW) potentials [33,34] with projectors up to $l = 1$ for H, $l = 2$ for Si, and $l = 3$ for Au are used. A number of 1 ($1s^1$), 4 ($3s^2 3p^2$), and 11 ($5d^{10} 6s^1$) valence electrons is employed for H, Si, and Au atoms, respectively. Plane waves up to an energy cutoff of 410 eV build up the basis for the expansion of the electronic wave functions. The silicon surfaces are modeled with asymmetric slabs consisting of 6 Si bilayers stacked along the [111] crystallographic direction, the surface termination including the Au chains, and a vacuum region of about 20 Å. H atoms saturate the dangling bonds at the opposite face of the slabs. These atoms as well as the three lowest Si bilayers are frozen at their bulk position to model the substrate, while the remaining atoms are free to relax. The atomic positions are relaxed until the residual Hellmann-Feynman forces are lower than 0.005 eV/Å. $4 \times 9 \times 1$ ($4 \times 27 \times 1$) Monkhorst-Pack k-point meshes [35] are employed to perform the energy integration in the Brillouin zone of the supercell of 5×6 (5×2) periodicity.

The calculated phonon eigenvalues depend strongly on the computational approach. Indeed, they depend both directly and indirectly (through the resulting structural differences) on the employed xc-functional. This is particularly true concerning the soft modes resulting from vibrations within the Au chain, which depend on the exact chain form. The form of the Au chain (quantified by its dimerization d_{Au}) and the relative stability of the investigated models within our approach are reported in Table I. To estimate the dependence of the phonon eigenvalues on the computational approach, we have calculated the vibrational frequencies of the double strand model as proposed by Krawiec [16] within the PBEsol [30], LDA [36,37] and GGA-PBE [38] approach.

According to the actual knowledge of the Si(553)-Au system, the D model is considered as a candidate for the description of the RT structure, while the SC, CSC, and R models are considered for the description of the LT phase. However, all the structures are modeled within DFT at 0 K and thermal lattice expansion is neglected.

While a limited number of surface localized phonons are experimentally detected, the frozen-phonon slab calculations lead to 246 vibrational modes for the double Au chain model by Krawiec [16] and 738 modes for the spin-polarized [9,25] and rehybridized models [26]. To achieve a comparison with the experimental results, we discard the phonons, whose atomic displacement vectors are localized by less than an arbitrarily chosen threshold of 40% in the two topmost atomic layers. This notwithstanding, the number of calculated phonon modes is still too high to allow for a frequency-based assignment of the calculated eigenmodes to the measured spectral features. To achieve this task, we compute the Raman scattering efficiency. Raman spectra are generated calculating the Raman susceptibility tensor as the first order derivative of the linear dielectric susceptibility tensor with respect to the atomic displacements. The computational approach is described in detail in Refs. [39,40] and recently applied to Si(111)-Au systems consisting of (5×2) Au wires [41] or ($\sqrt{3} \times \sqrt{3}$) planar reconstructions [42]. As the electronic structure is self-consistently calculated according to the phonon displacement, phonon induced charge transfer and modifications of the electronic band structure

TABLE I. Relative stability and Au chain dimerization calculated withtin DFT-PBEsol for the considered models. The dimerization is quantified as usual by the dimensionless parameter $d_{\mathrm{Au}} = (|a_{\mathrm{Au}} - a_{\mathrm{Si}}|)/a_{\mathrm{Si}}$, where a_{Si} is the surface lattice constant and a_{Au} is the Au-Au bond length in chain direction. E^{F} labels the formation energy in eV per 5×6 unit cell relative to the rehybridized model. Acronyms defined in Fig. 1.

	D [16]	SC [9]	CSC [25]	R [26]
d_{Au}	0.069	0.061	0.080	0.138
E^{F}	0.160	0.135	0.111	0.000

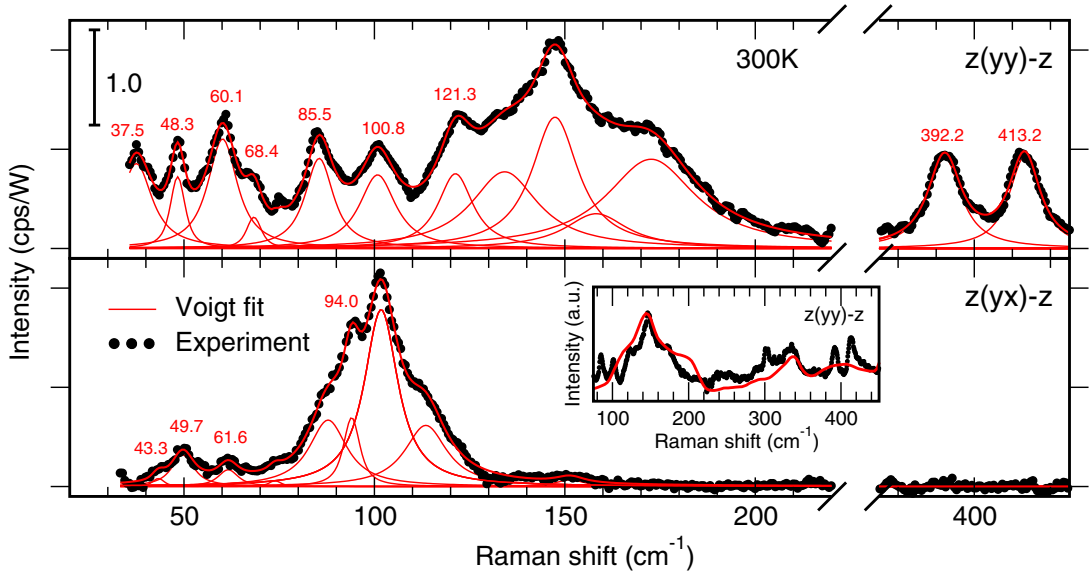

FIG. 2. Raman spectra of the Si(553)-Au surface after subtraction of the bulk scattering, measured at 300 K in the $z(yy)$-z and $z(yx)$-z polarization. The measured Raman spectra were fitted using Voigt profiles with Gauss FWHM fixed to the spectrometer resolution of 1.3 cm^{-1} and variable Lorentz FWHM. The inset shows a comparison of the measured Raman intensity with the PBEsol calculated phonon DOS of bulk Si.

are both accounted for. Theoretical spectra are constructed adding Lorentz functions centered at the calculated phonon frequencies, with height corresponding to the calculated Raman efficiency and experimental width. Spectra are calculated for an experimental laser photon energy of 1.91 eV, after consideration of the DFT underestimation of 0.5 eV of the fundamental band gap of the Si bulk.

B. Experimental Details

The Si(553) substrate was prepared from commercially available polished wafers. The sample was chemically cleaned ex-situ and then degassed in UHV for several hours. For the preparation of the Si(553)-Au-(5×2) reconstruction, the Si(553) substrate was exposed to several flashing steps up to 1150 °C. After deposition of 0.48 ML Au, which was monitored in real-time by reflection anisotropy spectroscopy (RAS), typical low-energy electron diffraction (LEED) patterns confirmed the growth quality and the long-range order of the metallic Au chains. Raman measurements were performed with a DILOR-XY triple spectrometer equipped with a high-efficiency Si-based CCD detector from ANDOR iDus. A Kr^+ laser was operated using the 647 nm (1.91 eV) line with a power of approximately 200 mW. The 647 nm laser is in resonance with optical transitions of the Si(553)-Au surface [21]. Thus, surface resonant Raman scattering is employed to enhance surface versus bulk Raman scattering efficiency [39]. The resolution of the spectrometer was determined from the width of the laser plasma lines to be 1.3 cm^{-1}. Through a helium closed-cycle cryostat from Advanced Research System, the sample was cooled down to a minimum temperature of 30 K. Stabilization of the sample at intermediate temperatures was obtained by combining the cryostat operation with a filament heating system using a PID control loop. Raman spectra of the Au-induced reconstruction are extracted subtracting the spectra of clean from that of the reconstructed surface. This methodology filters out bulk contributions from Si and provides only the surface-related spectrum, as demonstrated in previous works [42]. However, the subtraction procedure is affected by larger uncertainties where the bulk signal is particularly strong. For this reason, we focus on the spectral regions below 200 cm^{-1} and above 350 cm^{-1}, which have no overlap with the strong Raman peak related to the Si 2TA bulk mode. Calculations reveal that all the Au related phonon modes occurr in the investigated spectral region.

III. RESULTS AND DISCUSSION

A. Phonon modes at room temperature

Figure 2 shows the measured differential Raman spectrum of the Si(553)-Au surface for two different scattering geometries, indicated according to the Porto notation [43,44] by $z(yy)$-z (parallel polarization) and $z(yx)$-z (crossed polarization). The two scattering geometries lead to two rich and very distinct experimental spectra. The spectrum measured below 200 cm^{-1} in parallel polarization features several homogeneously distributed signatures of similar intensity and some minor peak. The broad feature observed between 110 and 200 cm^{-1} has been previously attributed to acoustic Si phonons activated by the Au superstructure [45]. Indeed, as shown in the inset of Fig. 2, the Raman signal in this region (black curve) strongly resembles the calculated phonon DOS of bulk Si (red curve), suggesting that bulk resonances dominate this spectral region. The nature and low surface localization of the modes theoretically predicted in this region confirm this interpretation.

The spectrum measured in crossed polarization shows peaks of small intensity at about 40, 50, and 60 cm^{-1}, and a dominating structured signature of large intensity centered at about 100 cm^{-1}. No signature is revealed above 120 cm^{-1}.

TABLE II. Raman frequencies (in cm^{-1}) measured at 300 K and calculated (0 K frozen phonon calculations performed with the D model) for the $z(yy)$-z configuration. The uncertainty in frequency is obtained from the Voigt line fit (with 90% confidence) and the error from the spectral calibration with laser plasma lines. PBEsol calculated frequencies are listed (Theo.), along with the highest and lowest frequency calculated with other XC-functionals. Char. and Loc. indicate whether the phonon has Au or Si character, and the surface localization of the atomic displacement vectors, respectively. Modes with calculated Raman efficiency below 1% of the main peak are not listed.

	Exp.	Theo.	Theo. Min-Max	Char.	Loc.
Low range	37.5 ± 0.3	35.4	35.1–36.4	Au	75%
		48.9	47.7–52.9	Au+Si	93%
	48.3 ± 0.1				
		52.7	52.7–59.8	Au	91%
	60.1 ± 0.1	64.9	64.9–66.5	Au+Si	68%
	68.4 ± 0.3	69.8	66.1–72.9	Au	92%
	85.5 ± 0.1	84.2	84.1–86.2	Au+Si	88%
	100.8 ± 0.2	109.4	109.4–113.1	Si	74%
	121.3 ± 0.4	122.0	122.0–129.4	Si	55%
	134.1 ± 1.4	131.9	131.8–141.1	Si	50%
	147.4 ± 0.7	140.2	140.2–144.0	Si	47%
	158.4 ± 4.7	165.1	165.1–167.5	Si	55%
	172.6 ± 1.9	169.8	169.7–171.3	Si	51%
High range	392.2 ± 0.1	386.2	379.8–388.3	Si	40%
	413.2 ± 0.1	411.5	410.1–415.7	Si	50%

The measured Raman spectra were fitted using Voigt profiles (indicated by red lines). The resulting experimental frequencies are listed in Tables II and III, and compared with calculated frequencies.

The vibrational properties of the Si(553)-Au system at 300 K are computed with the structural model proposed by Krawiec [16] [see Fig. 1(a)]. Although, according to recent investigations, the Si(553)-Au surface at 300 K oscillates between the D, R, and SC/CSC phases, the system is for the vast majority of the time in the D configuration [27], which is therefore employed to describe the high temperature phase of the Si(553)-Au surface.

TABLE III. Raman frequencies (in cm^{-1}) measured at 300 K and calculated (0 K frozen phonon calculations performed with the D model) for the $z(yx)$-z configuration. The uncertainty in frequency is obtained from the Voigt line fit (with 90% confidence) and the error from the spectral calibration with laser plasma lines. PBEsol calculated frequencies are listed (Theo.), along with the highest and lowest frequency calculated with other XC-functionals. Char. and Loc. indicate whether the phonon has Au or Si character, and the surface localization of the atomic displacement vectors, respectively. Modes with calculated Raman efficiency below 1% of the main peak are not listed.

	Exp.	Theo.	Theo. Min-Max	Char.	Loc.
Low range	43.3 ± 0.9	44.2	44.2–46.1	Au	58%
	49.7 ± 0.4	52.7	52.7–59.8	Au	91%
	61.6 ± 0.5	62.4	61.7–64.6	Au	91%
	73.9 ± 1.1	65.4	65.4–67.6	Si	47%
	87.4 ± 0.9	79.7	79.7–86.2	Si	57%
		82.1	82.1–86.1	Au	77%
	94.0 ± 0.2				
		84.4	84.4–94.9	Au	77%
	101.7 ± 0.2	96.8	96.2–98.8	Au	72%
	113.5 ± 0.5	111.4	111.4–115.3	Si	52%

Among the calculated phonon modes a considerable fraction is Raman silent. The calculated phonon spectra, shown in Fig. 3, closely reproduce the measured spectra. Solely the peaks of moderate intensity predicted at about 150 cm^{-1} in the crossed polarization are not experimentally observed. However, the assignment of phonon modes in this spectral region is difficult because of the overlap with broad and intense bulk phonons. Generally, both the frequency and the relative intensity of the spectral features are in satisfactorily agreement with the experiment, although the most intense vibrational signatures in the (yx) crossed configuration are somewhat red shifted within PBEsol in comparison with the experiment. The good agreement between measured and calculated spectra allows to assign the calculated phonon displacement patterns on the basis of energy, symmetry, and Raman intensity. The result of this procedure is shown in Tables II and III.

Selected displacement patterns of Raman active modes are represented in Figs. 4 and 5. In these pictures, upwards and downwards vertical displacements are represented by dots and crosses, respectively. The calculated displacement patterns reflect the polarization dependence of the Raman spectra. The modes detectable in parallel polarization are symmetric with respect to the mirror symmetry plane perpendicular to the Au wires shown in Figs. 4(d) and 5(d). The modes that are Raman active in crossed polarization do not possess this symmetry. This relationship between selection rules and phonon symmetry is valid, assuming deformation potentials as the origin of the Raman scattering.

More in detail, in the crossed configuration six modes are clearly visible, along with low intensity signatures. All the corresponding displacement patterns, shown in in Fig. 4 break the local symmetry of the terrace, as expected for modes that are Raman active in crossed polarization. The tiny feature predicted at 44.2 cm^{-1} [Fig. 4(a), at 43.3 cm^{-1} in the experiment] is a rigid translation of the Au chain. The first pronounced feature, predicted at 52.7 cm^{-1}, is due to a seesaw movement within the Au chain, as shown in Fig. 4(b). The second pronounced Raman peak, which appears as a single feature at about 61 cm^{-1} in the measured spectra, is due to the overlap of two modes at 62.4 and 65.4 cm^{-1}, represented in Figs. 4(c) and 4(d), respectively. The modes at 65.4 and 79.7 cm^{-1} describe a rigid translation and the shear movement of the honeycomb chain [Fig. 4(e)]. These modes are the energetically lowest Si surface modes. A lateral shear movement within the Au chain [Fig. 4(f)] is the displacement pattern of the phonon predicted at 82.1 cm^{-1}. The mode at 84.4 cm^{-1} shown in Fig. 4(g) is a torsion within the Au chain, while the mode at 96.8 cm^{-1} shown in Fig. 4(h) is another distortion of the Au chain. Further modes of moderate intensities at higher frequencies are not experimentally observed (due to the overlap with bulk resonances) and will not be discussed in detail.

In parallel polarization, more modes are visible. While at lower frequencies the Au related modes dominate, above

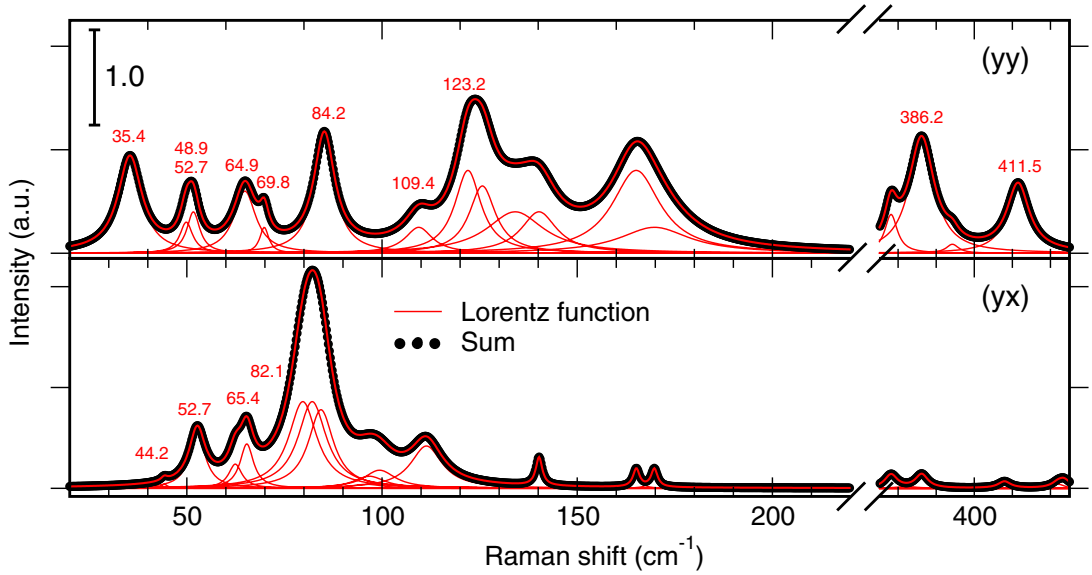

FIG. 3. Raman spectra of the Si(553)-Au surface calculated within DFT-PBEsol for the (*yy*) and (*yx*) polarization with the structural model by Krawiec *et al.* [16].

100 cm^{-1} only Si modes are found. This is expected, due to the much higher mass of the Au atoms with respect to Si. The mode at 35.4 cm^{-1} in Fig. 5(a) is a vertical rigid shift of the Au chain, corresponding to the first measured peak at 37.5 cm^{-1}. The second Raman feature measured at 48.3 cm^{-1} is the overlap of two close phonons at 48.9 and 52.7 cm^{-1}, with similar displacement pattern, represented in Fig. 5(b). Both modes perform the same seesaw movement within the Au-chain, however, the first one features a more pronounced in-phase movement of the step edge, which increases the phonon effective mass and lowers its frequency.

These two modes couple Au chain and Si step edge, and are associated to charge transfer between different regions of the Si(553) terrace. They deserve a more detailed description, as they break the local terrace symmetry and should not be Raman active in parallel polarization, assuming deformation potentials as the origin of the Raman scattering. However, a further Raman mechanism—scattering at charge density fluctuations—must be considered for these modes. Charge fluctuations between the step edge and the Au chain occur when atomic displacements modify the Au-Au bond length and the relative height of the step edge atoms, as revealed by previous studies [20,21,27]. Scattering at charge density fluctuations, which is well known, e.g., for highly doped semiconductors [46] is traced to the modifications of the adsorption edge due to the phonon-induced charge redistribution and had not been previously observed for quasi-1D systems. This mechanism contributes to the Raman scattering only in parallel configuration and occurs for all modes associated with strong charge fluctuations. Yet, it is generally difficult to distinguish and quantify the relative contributions of scattering at charge density fluctuations and deformation potentials to the total Raman intensity, as both occur in parallel polarization. However, for the mode in Fig. 5(b), no deformation potential scattering can take place in parallel polarization, due to the phonon symmetry. Therefore, only scattering at charge density fluctuations can be responsible for the Raman intensity of this mode.

We assigned the feature measured at 48.3 cm^{-1} in parallel polarization and to the feature at 49.7 cm^{-1} in crossed polarization, to the same displacement pattern as discussed above, suggesting that both signatures are due to the same phonon but different scattering mechanisms. Further peaks of similar energies in parallel and crossed polarization are assigned to different phonon modes on the basis of the calculated intensities, instead.

The phonon at 64.9 cm^{-1} [Fig. 5(c)] is a rigid vertical translation of Au and HC chains, which modifies their relative height. The mode at 69.8 cm^{-1} in Fig. 5(d) couples the dimers within the Au chain. At 84.2 cm^{-1} we predict an in-phase tilting of the Au and HC chain along the chain axes [Fig. 5(e)]. At higher frequencies, Si related modes become dominant. A rotation mode of the honeycombs [Fig. 5(f)] occurs at 109.4 cm^{-1}, further modes at 123.1 and 169.8 cm^{-1} are different vertical displacements within the HC chain. We remark that the theoretically predicted Raman scattering efficiency of the modes in this spectral region is much lower than the measured intensity, which has a strong contribution from Au activated bulk modes, as shown in the inset of Fig. 2.

In the high frequency range (i.e., above 350 cm^{-1}), two phonon modes at 392 cm^{-1} and 413 cm^{-1}, previously attributed to Si step edge vibrations [27,45] are observed only in the parallel scattering geometry (Figs. 2 and 3). Our models confirm this interpretation. The corresponding displacement patterns are shown in Fig. 5(g) and 5(h), respectively. The first peak, predicted at 386.2 cm^{-1}, is assigned a movement of the left part of HC chain. Instead, the second peak at 411.5 cm^{-1} can be clearly assigned to a transversal shear mode along the Si honeycomb chain, confirming a previous assignment [27].

The close agreement between the theoretical and experimental results strongly suggests that the double Au strand model [16] correctly describes the Si(553)-Au system.

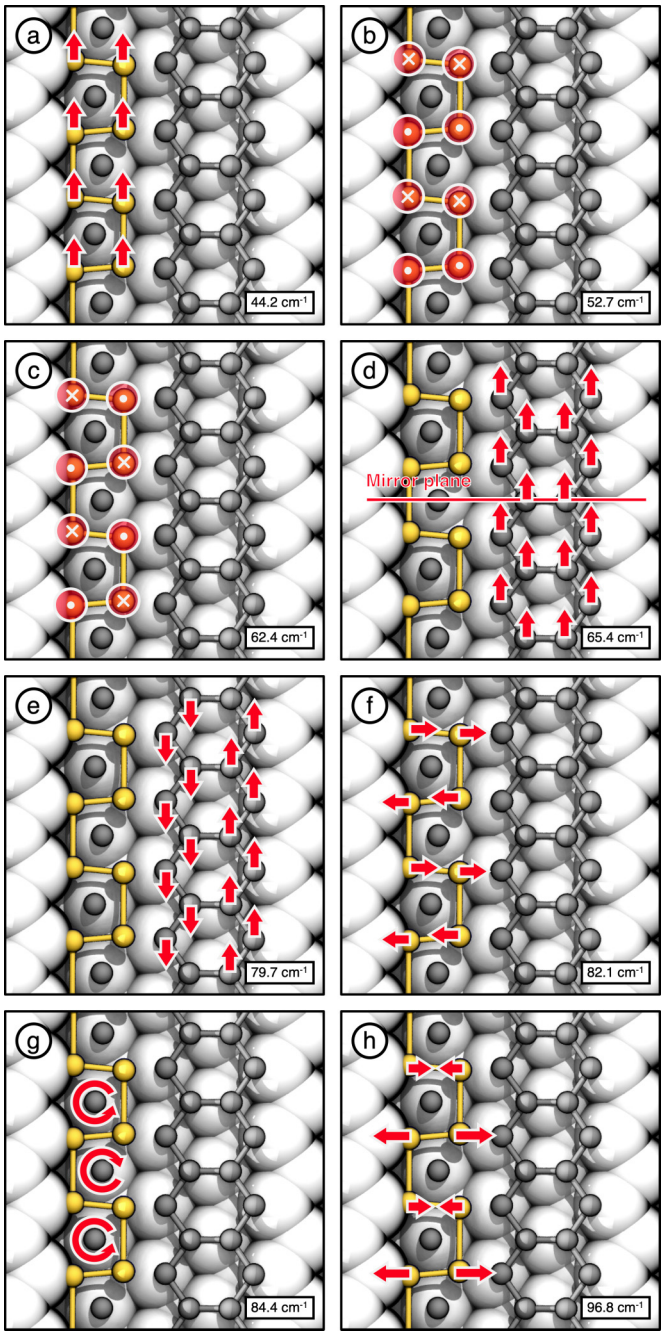

FIG. 4. Schematic representation of the displacement pattern of selected phonon modes that are Raman active in the crossed polarization. The displacement patterns are calculated within DFT-PBEsol according to the double Au strand model [16] of the RT phase.

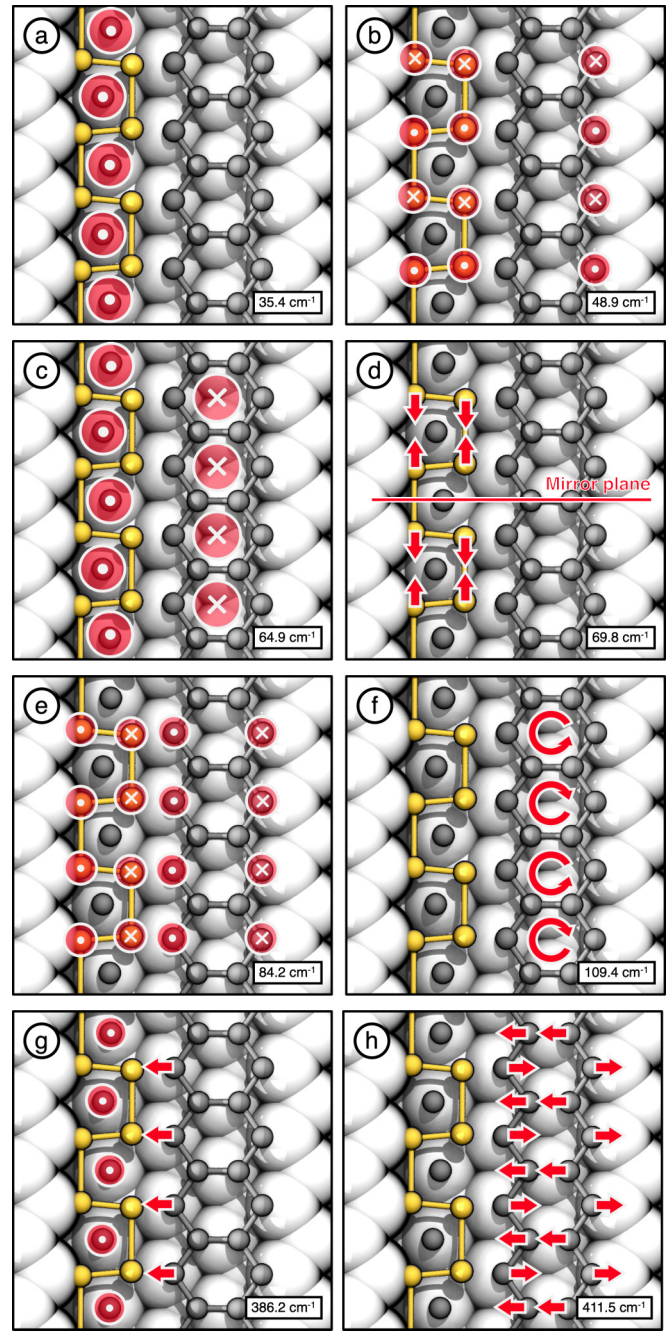

FIG. 5. Schematic representation of the displacement pattern of phonon modes that are Raman active in the parallel polarization. The displacement patterns are calculated within DFT-PBEsol according to the double Au strand model [16] of the RT phase.

B. Phonon modes below and above the phase transition

The Si(553)-Au system is supposed to undergo an order-disorder type structural transition starting below 100 K [27]. According to the actual knowledge of the system, the double Au strand model of (5×2) periodicity[16] describes the high symmetric RT phase, while the (centered) spin-chain [9,25] and rehybridized [26] models of (5×6) periodicity have been proposed for the description of the lower symmetric LT phase. Between RT and LT the morphology of the step edge of the Si terraces fluctuates among the configurations of the two phases, establishing an interplay (via charge transfer) with the Au chain that continuously enhances the chain dimerization from RT to LT [27].

The different symmetry of the two phases must be mirrored in their vibrational properties. In particular, modes associated with the Au chain are expected to modify their frequency from RT to LT, while modes localized at the Si step edge cannot exist in the same form in the two phases. To verify this assumption, we have investigated the phonon spectrum well below and well above the transition temperature. As the

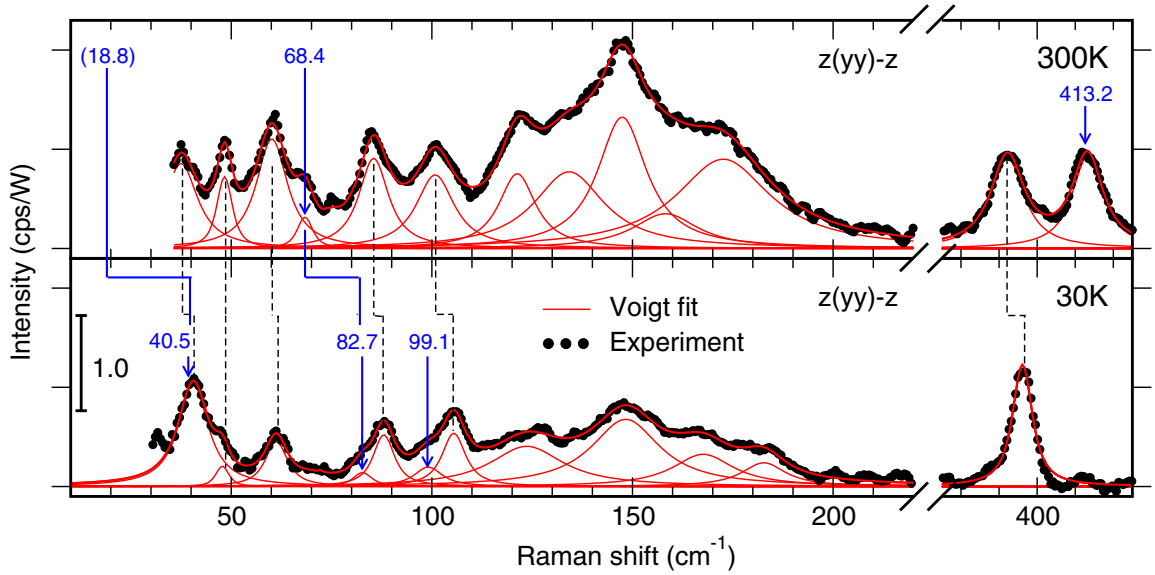

FIG. 6. Raman spectra of the Si(553)-Au surface after subtraction of the bulk scattering, measured at 300 K and 30 K in parallel polarization. The measured Raman spectra were fitted using Voigt profiles with Gauss FWHM fixed to the spectrometer resolution of 1.3 cm^{-1} and variable Lorentz FWHM. Blue arrows mark features with strong temperature dependence, while dotted black lines join features observed at both temperatures.

RT and LT structural models differ in the dimerization of the Au chain and in the form of the Si step edge, we focus on the frequency ranges in which the vibrations related to the Au chain and to the Si step edge occur. As predicted by theory, these are below 100 cm^{-1} and above 380 cm^{-1}, respectively. The spectral region in between is furthermore characterized by very broad features, which are less well suited for a precise estimation of the temperature shifts.

The LT Raman spectra of Si(553)-Au are shown in Fig. 6, along with the RT spectra for comparison. The Raman peaks RT and LT are joined as suggested by the calculations discussed in the following. The experimental frequencies at RT and LT are summarized in Table IV. The modes at 68.4 and 413.2 cm^{-1} (assigned to distortions of the Au chain and of the step edge) are only observed at RT, while modes at 82.7 and 99.1 cm^{-1} are exclusive to LT.

TABLE IV. Measured Raman frequencies at 300 and 30K in the *z*(*yy*)-*z* scatteing geometry. The uncertainty in frequency is obtained from the Voigt line fit (with 90% confidence) and the error from the spectral calibration with laser plasma lines.

	Exp. 300 K	Exp. 30 K	Diff.
Low range	37.5 ± 0.4	40.5 ± 0.2	3.0
	48.3 ± 0.2	47.8 ± 0.4	−0.5
	60.7 ± 0.3	61.2 ± 0.2	0.4
	68.4 ± 0.4	–	
	–	82.7 ± 1.4	
	85.5 ± 0.3	88.0 ± 0.4	2.5
	–	99.1 ± 1.5	
	100.8 ± 0.2	105.5 ± 0.4	4.7
High range	392.2 ± 1	396.2 ± 1	4.0
	413.2 ± 1	–	

To understand the changes in the measured spectra, the vibrational properties of the Si(553)-Au system at LT have been calculated with all structural models that have been proposed in the literature for the description of this phase, namely the spin-chain [9] and centered spin-chain model [25], as well as the rehybridized model [26]. Unfortunately, the calculation of the Raman scattering efficiency for the LT structural models is an exceptionally demanding task, due to both system size and number of phonons (396 atoms and 738 vibrational modes for each structure). However, the knowledge of the calculated Raman frequencies and displacement patterns can still be used to interpret the experimental data.

The comparison of the displacement patterns and corresponding eigenfrequencies calculated with the RT and LT models allows to discriminate three categories of phonons: modes which are common to the RT and LT phases, modes that occur both in the RT and in the LT phase, however with a different frequency, and modes that exist either only in the RT or only in the LT structure. Most of the frequencies calculated with the RT model can be identified in all three candidate models within a few cm^{-1}. However, important exceptions are found in the experimentally investigated range, corresponding exactly to the measured LT-RT differences.

The first deviation is represented by the Au dimerization mode shown in Fig. 7(a), which exists in both the RT and LT structure, yet at different frequencies. This mode is predicted at 18.8 ± 5 cm^{-1} with the RT model, and is thus not experimentally accessible. However, it becomes much harder (42.0 cm^{-1}) within the rehybridized model, which features a more pronounced dimerization, as noted in Table I. As this mode shortens the Au-Au bond length, it requires more energy for a strongly dimerized Au chain. In the experimental spectrum, a noticeable peak shift from 37.5 to 40.5 cm^{-1} is observed in this energy region between 300 K and 30 K along with a strong increase of the Raman intensity. Yet, this

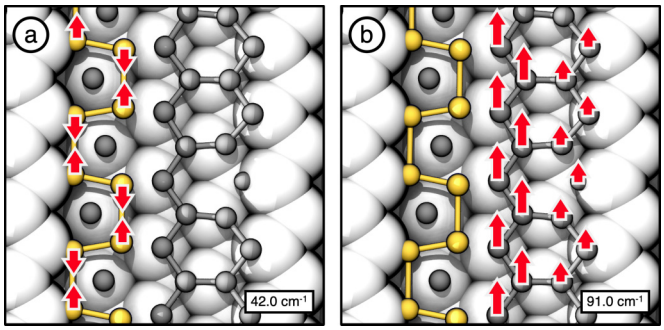

FIG. 7. Schematic representation of the displacement pattern of the dimerization mode and of the honeycomb translation mode. The displacement patterns are calculated within DFT-PBEsol according to the rehybridized model [26] of the LT phase.

is surprising, as the peak at 37.5 cm^{-1} [vertical translation of the Au chain, Fig. 5(a)] is not expected to be affected by temperature. Indeed, theory predicts a small shift of about 1.5 cm^{-1} in the opposite direction for this mode. This suggests that the peak observed at LT at 40.5 cm^{-1} is the overlap of a weakly temperature-dependent mode at 37.5 cm^{-1} and the dimerization mode at about 42 cm^{-1}. This would both explain the observed modifications in intensity and frequency, and also be in agreement with a previous interpretation [27].

The second exception is represented by a further mode with strong frequency shift, the mode calculated at 69.8 cm^{-1} shown in Fig. 5(d). Similarly to the dimerization mode, this mode shortens the Au-Au bond length and becomes much harder by about 8 cm^{-1} for the rehybridized model. This mode is associated to the low-intensity peak at 68.4 cm^{-1} at high temperatures, which seems to disappear at 30 K. Comparison with theory suggests that this mode shifts at higher frequencies and can be assigned the mode at about 82.7 cm^{-1} which is not observed in the RT Raman spectrum.

Another difference between the HT and LT phase is the appearence of the feature at 99.1 cm^{-1} in the measured LT spectra, which we associate to the displacement pattern calculated with the rehybridized model and displayed in Fig. 7(b). At LT, this mode is visible in the parallel polarization Raman spectrum via charge density fluctuation scattering, according to its symmetry. This mode is not existent in the RT structure, but closely related to the chain translation modes predicted at 65.4 cm^{-1} and at 79.7 cm^{-1} [Figs. 4(d) and 4(e)] at RT, which are visible via deformation potential scattering in the crossed polarization Raman spectrum. This mode is a translation of the HC chain, which strongly hindered by the LT modification of the step edge pinning the outer atoms and therefore making this mode much harder.

Finally, the mode measured at 413 cm^{-1} and associated to the theoretically predicted step edge mode at 411.5 cm^{-1} [see Fig. 5(h)] is only a phonon mode of the RT phase. Due to the different symmetry of the Si step edge in the structural models associated to the LT and RT phases, this lattice vibration has no low temperature counterpart. In the rehybridized model, this mode is decomposed into local vibrations of the step edge, as previously pointed out by Braun *et al.* [27].

TABLE V. Raman frequencies (in cm^{-1}) of selected modes discussed in the text calculated within PBEsol according to different structural models.

Exp.	R	SC	CSC
40.5 ± 0.2	42.0	8.7	16.7
82.7 ± 1.4	77.3	69.4	70.7
99.1 ± 1.5	91.0	65.0	64.8

To summarize, the rehybridized model can well explain the observed temperature shifts. On the contrary, in the (centered) spin-chain model [9,25] the dimerization is not as pronounced as in the rehybridized model [26] and therefore the frequency shifts with respect to the high temperature model cannot be reproduced. For example, the dimerization mode [see Fig. 7(a), and Table V] is predicted by DFT-PBEsol at 8.7 and 16.7 cm^{-1}, for the spin-chain and centered spin-chain models, respectively. This value is far from the value of 42.0 cm^{-1} calculated with the rehybridized model and assigned to the peak measured at 40.5 cm^{-1}. Similarly, the mode that couples the Au dimers [see Fig. 5(d)] calculated at 68.9 cm^{-1} for the RT structure, does not significantly shift at LT in the SC and CSC model (69.4 and 70.7 cm^{-1}, respectively) and cannot explain the spectral feature measured at 82.7 cm^{-1}. Thus, the comparison of the calculated vibrational properties with the measured spectra yields a strong argument for the rehybridized model for the description of the low-temperature phase.

IV. CONCLUSION

The phonon spectrum of the Si(553)-Au surface has been studied above and below the phase transition by Raman spectroscopy and DFT-based atomistic calculations. The latter reproduced satisfactorily the measured spectra, if the double Au strand model and the rehybridized model are used for the simulation of the RT and LT phase, respectively. The agreement between measured and calculated data allows us to propose an assignment of the mode-specific phonon displacement patterns to the spectral signatures. Furthermore, a pronounced temperature dependence of different modes (at 40.5 and 99 cm^{-1} in the LT phase and at 68.4 and 413 cm^{-1} in the RT phase) is interpreted as a signature of a structural phase transition. As a general feature, modes that modify the Au-Au bond length and modes localized at the Si step edge are significantly influenced by the phase transition.

The analysis of the phonon displacement patterns reveals that the transversal Au-related modes as the mode predicted at LT at 42.0 cm^{-1} are the fingerprints of the dimerization. The experimentally observed large frequency shift of these modes with temperature shows that the dimerization is significantly affected during the phase transition due to charge transfer between Au- and Si-related surface states.

Modes which involve the Si step edge atoms either disappear or are shifted to much higher energies at LT. In particular, the mode predicted at 411.5 cm^{-1}, associated to transversal vibrations of the Si step edge, disappears at LT, where ther-

mal fluctuations are frozen and the surface structure shows a higher order.

The phonon activated charge transfer between the Au chain and the Si step edge, which is responsible for the observed order-disorder phase transition [27], leads to Raman scattering by charge density fluctuations. This mechanism renders Raman active the modes coupling the Au dimer rows and the Si step edge, although they should be Raman silent due to the symmetry of their displacement pattern. This allows for a direct observation of the strong coupling between electronic and phononic systems on the Si(553)-Au surface.

Summarizing, the phonon spectra of the Si(553)-Au at different temperatures show pronounced differences that we interpret as a signature of a structural phase transition. We propose an assignment of the peaks which is exploited to assign a structural model to the LT and the RT phases. The knowledge of the vibrational properties of the Si(553)-surface is moreover a prerequisite for future investigation of structural modifications as induced to modify the coupling with higher dimensions.

ACKNOWLEDGMENTS

We gratefully acknowledge financial support from the Deutsche Forschungsgemeinschaft (research unit FOR1700, Projects No. SA 1948/1-2 and No. Es 127/12-2, and FOR2824, Project No. SA 1948/2-1). Financial support by the Ministerium für Kultur und Wissenschaft des Landes Nordrhein-Westfalen, Der Regierende Bürgermeister von Berlin, Senatskanzlei Wissenschaft und Forschung, and the Bundesministerium für Bildung und Forschung is acknowledged. Calculations for this research were conducted on the Lichtenberg high-performance computer of the TU Darmstadt and at the Höchstleistungrechenzentrum Stuttgart (HLRS). The authors furthermore acknowledge the computational resources provided by the HPC Core Facility and the HRZ of the Justus-Liebig-Universität Gießen.

[1] S. Kagoshima, H. Nagasawa, and T. Sambongi, *One-Dimensional Conductors*, Springer Series in Solid-State Sciences (Springer, Berlin, 1988), Vol. 72, pp. 126–135.
[2] G. Grüner, Rev. Mod. Phys. **60**, 1129 (1988).
[3] J. M. Luttinger, J. Math. Phys. **4**, 1154 (1963).
[4] K. Schönhammer, Luttinger liquids: Basic concepts, in *Strong Interactions in Low Dimensions*, Physics and Chemistry of Materials with Low-Dimensional Structures, edited by L. D. D. Baeriswyl (Springer Netherlands, Dordrecht, 2004), Chap. 4, Vol. 25, pp. 93–136.
[5] T. Giamarchi, *Quantum Physics in One Dimension* (Clarendon Press, Oxford, 2007).
[6] C. Zeng, P. Kent, T.-H. Kim, A.-P. Li, and H. H. Weitering, Nat. Mater. **7**, 539 (2008).
[7] P. C. Snijders and H. H. Weitering, Rev. Mod. Phys. **82**, 307 (2010).
[8] H. Weitering, Nat. Phys. **7**, 744 (2011).
[9] S. C. Erwin and F. J. Himpsel, Nat. Commun. **1**, 58 (2010).
[10] J. Aulbach, J. Schäfer, S. C. Erwin, S. Meyer, C. Loho, J. Settelein, and R. Claessen, Phys. Rev. Lett. **111**, 137203 (2013).
[11] C. Brand, H. Pfnür, G. Landolt, S. Muff, J. H. Dil, T. Das, and C. Tegenkamp, Nat. Commun. **6**, 8118 (2015).
[12] K. Holtgrewe, S. Appelfeller, M. Franz, M. Dähne, and S. Sanna, Phys. Rev. B **99**, 214104 (2019).
[13] J. N. Crain, J. L. McChesney, F. Zheng, M. C. Gallagher, P. C. Snijders, M. Bissen, C. Gundelach, S. C. Erwin, and F. J. Himpsel, Phys. Rev. B **69**, 125401 (2004).
[14] I. Barke, F. Zheng, T. K. Rügheimer, and F. J. Himpsel, Phys. Rev. Lett. **97**, 226405 (2006).
[15] J. Aulbach, S. C. Erwin, R. Claessen, and J. Schäfer, Nano Lett. **16**, 2698 (2016).
[16] M. Krawiec, Phys. Rev. B **81**, 115436 (2010).
[17] I. Miccoli, F. Edler, H. Pfnür, S. Appelfeller, M. Dähne, K. Holtgrewe, S. Sanna, W. G. Schmidt, and C. Tegenkamp, Phys. Rev. B **93**, 125412 (2016).
[18] C. Braun, C. Hogan, S. Chandola, N. Esser, S. Sanna, and W. G. Schmidt, Phys. Rev. Mater. **1**, 055002 (2017).
[19] F. Edler, I. Miccoli, J. P. Stöckmann, H. Pfnür, C. Braun, S. Neufeld, S. Sanna, W. G. Schmidt, and C. Tegenkamp, Phys. Rev. B **95**, 125409 (2017).
[20] Z. Mamiyev, S. Sanna, T. Lichtenstein, C. Tegenkamp, and H. Pfnür, Phys. Rev. B **98**, 245414 (2018).
[21] C. Hogan, E. Speiser, S. Chandola, S. Suchkova, J. Aulbach, J. Schäfer, S. Meyer, R. Claessen, and N. Esser, Phys. Rev. Lett. **120**, 166801 (2018).
[22] M. Tzschoppe, C. Huck, F. Hötzel, B. Günther, Z. Mamiyev, A. Butkevich, C. Ulrich, L. Gade, and A. Pucci, J. Phys. Condens. Matter **31**, 195001 (2018).
[23] S. Polei, P. C. Snijders, S. C. Erwin, F. J. Himpsel, K.-H. Meiwes-Broer, and I. Barke, Phys. Rev. Lett. **111**, 156801 (2013).
[24] S. Polei, P. C. Snijders, K.-H. Meiwes-Broer, and I. Barke, Phys. Rev. B **89**, 205420 (2014).
[25] B. Hafke, T. Frigge, T. Witte, B. Krenzer, J. Aulbach, J. Schäfer, R. Claessen, S. C. Erwin, and M. Horn-von Hoegen, Phys. Rev. B **94**, 161403(R) (2016).
[26] C. Braun, U. Gerstmann, and W. G. Schmidt, Phys. Rev. B **98**, 121402(R) (2018).
[27] C. Braun, S. Neufeld, U. Gerstmann, S. Sanna, J. Plaickner, E. Speiser, N. Esser, and W. G. Schmidt, Phys. Rev. Lett. **124**, 146802 (2020).
[28] F. Edler, I. Miccoli, H. Pfnür, and C. Tegenkamp, Phys. Rev. B **100**, 045419 (2019).
[29] B. Hafke, C. Brand, T. Witte, B. Sothmann, M. Horn-von Hoegen, and S. C. Erwin, Phys. Rev. Lett. **124**, 016102 (2020).
[30] J. P. Perdew, A. Ruzsinszky, G. I. Csonka, O. A. Vydrov, G. E. Scuseria, L. A. Constantin, X. Zhou, and K. Burke, Phys. Rev. Lett. **100**, 136406 (2008).
[31] G. Kresse and J. Furthmüller, Comput. Mater. Sci. **6**, 15 (1996).
[32] G. Kresse and J. Furthmüller, Phys. Rev. B **54**, 11169 (1996).
[33] G. Kresse and D. Joubert, Phys. Rev. B **59**, 1758 (1999).
[34] P. E. Blöchl, Phys. Rev. B **50**, 17953 (1994).
[35] H. J. Monkhorst and J. D. Pack, Phys. Rev. B **13**, 5188 (1976).

[36] D. M. Ceperley and B. J. Alder, Phys. Rev. Lett. **45**, 566 (1980).
[37] J. P. Perdew and A. Zunger, Phys. Rev. B **23**, 5048 (1981).
[38] J. P. Perdew, K. Burke, and M. Ernzerhof, Phys. Rev. Lett. **77**, 3865 (1996).
[39] E. Speiser, N. Esser, B. Halbig, J. Geurts, W. G. Schmidt, and S. Sanna, Surf. Sci. Rep. **75**, 100480 (2020).
[40] S. Sanna, S. Neufeld, M. Rüsing, G. Berth, A. Zrenner, and W. G. Schmidt, Phys. Rev. B **91**, 224302 (2015).
[41] M. Liebhaber, B. Halbig, U. Bass, J. Geurts, S. Neufeld, S. Sanna, W. G. Schmidt, E. Speiser, J. Räthel, S. Chandola, and N. Esser, Phys. Rev. B **94**, 235304 (2016).
[42] B. Halbig, M. Liebhaber, U. Bass, J. Geurts, E. Speiser, J. Räthel, S. Chandola, N. Esser, M. Krenz, S. Neufeld, W. G. Schmidt, and S. Sanna, Phys. Rev. B **97**, 035412 (2018).
[43] T. C. Damen, S. P. S. Porto, and B. Tell, Phys. Rev. **142**, 570 (1966).
[44] C. A. Arguello, D. L. Rousseau, and S. P. S. Porto, Phys. Rev. **181**, 1351 (1969).
[45] E. Speiser, J. Plaickner, S. Chandola, N. Esser, B. Halbig, and J. Geurts, Physica Status Solidi (b) **256**, 1800341 (2019).
[46] G. Abstreiter, M. Cardona, and A. Pinzcuk, Light Scattering by free carrier excitations in semiconductors, in *Light Scattering in Solids IV: Electronic Scattering, Spin Effects, SERS and Morphic Effects*, edited by M. Cardona and G. Güntherodt, Topics in Applied Physics (Springer Verlag, Berlin, 1984), Vol. 54.